Density of Uranus moons: Evidence for ice/rock fractionation during planetary accretion

Bruno Reynard, Christophe Sotin

To cite this version:

Bruno Reynard, Christophe Sotin. Density of Uranus moons: Evidence for ice/rock fractionation during planetary accretion. Icarus, 2025, 425, pp.116354. 10.1016/j.icarus.2024.116354 . hal-04868706

HAL Id: hal-04868706
https://hal.science/hal-04868706v1

Submitted on 6 Jan 2025

Density of Uranus moons: evidence for ice/rock fractionation during planetary accretion

Bruno Reynard[1*], Christophe Sotin[2]

[1]Univ Lyon, ENS Lyon, UCB Lyon 1, Univ St-Etienne, CNRS, Laboratoire de Géologie de Lyon, 69007 Lyon, France

[2]Laboratoire de Planétologie et Géosciences, Nantes Université, Univ Angers, Le Mans Université, CNRS, UMR 6112, F-44000 Nantes, France

*corresponding author name(s) here.

Email: bruno.reynard@ens-lyon.fr

Author Contributions: Authors contributed equally to the article.

Competing Interest Statement: Authors declare that they have no competing interests.

Abstract. Current models suggest the five regular moons of Uranus formed in a single stage from a primary planetary disk or a secondary impact disk. Using latest estimates of moon masses (Jacobson, 2014), we find a power-law relationship between size and density of the moons due to varying rock/ice ratios caused by fractionation processes. This relationship is better explained by mild enrichment of rock with respect to ice in the solids that aggregate to form the moons following Rayleigh law for distillation (Rayleigh, 1896) than by differential diffusion in the disk, although the two mechanisms are not exclusive. Rayleigh fractionation requires that moon composition and density reflect their order of formation in a closed-system circumplanetary disk. For Uranus, the largest and densest moons Titania and Oberon (R ~ 788 and 761 km, respectively) first formed, then the mid-sized Umbriel and Ariel (585 and 579 km), satellites in each pair forming simultaneously with similar composition, and finally the small rock-depleted Miranda (236 km). Fractionation likely occurred through impact vaporization during planetesimal accretion. This mechanism would add to those affecting the composition of accreting planets and moons in disks such as temporal/spatial variation of disk composition due to temperature gradients, advection, and large impacts. In the outer solar nebula, Rayleigh fractionation may account for the separation of a rock-dominated reservoir, and an ice-dominated reservoir, currently represented by CI carbonaceous chondrite/type-C asteroids and comets, respectively. Potential consequences for Uranus moons' composition are discussed.

1. Introduction

Uranus' regular moons attract attention as targets for future spatial missions because they may host internal oceans (Bierson and Nimmo, 2022; Castillo-Rogez et al., 2023; Hussmann et al., 2006). They are also a unique system because models have suggested they may form in a single stage from a primary spreading disk (Szulágyi et al., 2018). The disk may have formed from ejected material after the impact of Uranus by a rocky planet several times the mass of the Earth that caused the tilt of the spin axis of Uranus and its moons (Kegerreis et al., 2018; Kurosaki and Inutsuka, 2019; Reinhardt et al., 2020; Slattery et al., 1992). Uranian moons formed in a few tens of millennia according to recent models of disk spreading and condensation (Ida et al., 2020; Woo et al., 2022). Alternative scenarios involve collisionless tilting due to the orbital destabilization of a heavy external moon that was lost either by ejection or collision with Uranus (Boué and Laskar, 2010; Saillenfest et al., 2022). With the density of regular moons increasing with increasing orbital semi-axis (Fig. 1), the Uranian system may provide fundamental information on the processes at work during condensation and aggregation of solids that eventually form bodies, both moons and planets, from spreading disks.

The Uranian satellite density increases with increasing distance to the planet, opposite to the trend in the Jovian system (Fig. 1a). Density variations are due to variations of the rock/ice ratio. The Jovian pattern could be due, among others, to the inhibition of ice accretion below the snow line in the circum-Jovian disk (Ronnet et al., 2017), or to tidal heating (Canup and Ward, 2009). The Saturnian system is characterized by one large moon (Titan) distant from the planet, and several smaller moons whose total mass only represents 4% of Titan’s mass, at the semblance of the initial configuration postulated for Uranus in non-collisional tilting scenarios with one large distant moon (Boué and Laskar, 2010; Saillenfest et al., 2022). Saturnian moon density shows however no regular pattern with semi-axis, suggesting a complex formation history (Charnoz et al., 2011; Neveu and Rhoden, 2019), possibly involving large impacts during Titan's accretion (Asphaug and Reufer, 2013).

A required ingredient in modeling the density of Uranian moons is the mixing of ice and refractory components (Castillo-Rogez et al., 2023; Hussmann et al., 2006). Condensation of silicate and ice take place at different temperatures, hence location in the spreading disk, leading to potential differences in the rock to ice ratio and density of the moons (Woo et al., 2022). Here we investigate what mechanism could account for a regular relationship found between Uranian satellite density and size (Fig. 1b). We propose that Rayleigh distillation due to fractionation of rock and ice during aggregation of the moons is a viable one. Consequences for composition of Uranus moons and multiphase objects forming in spreading disks are discussed.

2. Size, density, and composition of Uranus regular moons

Uranus regular moon densities (Table 1) show a power-law relationship between the moon density and size (Fig. 1b). The relationship is solid because it holds when established only from the density of the four largest moons, and predicts within uncertainties the density of Miranda that represents only 0.7% of the total mass of the satellites. It is worth noting that the four largest moons form two pairs of similar density and size, Oberon-Titania accounting for 71% of the total mass, thus there are three distinct density-radius values. There is no indication of a correlation in the determination of moon masses that could lead to such a relationship (Jacobson, 2014). The average density of Uranus moons (1616 km/m^3) is consistent with that of carbon-rich "solar" composition defined from mineralogical and density-moment of inertia modeling of icy moons and dwarf planets (Reynard and Sotin, 2023).

Constraints on the composition and internal structure of the moons are given by their mass (Jacobson, 2014), size and shape (Thomas, 1988). Elongation of Miranda and Ariel along their suburanian equatorial radius (Thomas, 1988) suggests they are differentiated into at least two layers, an icy hydrosphere and a refractory core (Castillo-Rogez et al., 2023) , hence that a global melting occurred. Umbriel, Titania and Oberon are of similar size or larger, and also differentiated owing to higher heat production from radioactive decay and higher temperatures (Hussmann et al., 2006). Based on tidal modeling, Mimas, a moon of Saturn that has very similar size and tidal parameters to Miranda, is predicted to host an extensive ocean at present time (Lainey et al., 2024). Applying this model to Miranda (Im(k2) $= -10^{-3}$), and using an eccentricity of 0.03 during a recent 5:3 resonance between Ariel and Umbriel on Miranda (Ćuk et al., 2020), we obtain a heat flux of ~50 mW/m^2, consistent with estimates based on the relaxation of a young corona (Beddingfield et al., 2022). The internal heating due to tidal dissipation is about ~10^{-6} W/kg, which would give a heating rate dT/dt of ~10 K/My, and extensive ice melting within a few tens of My. Tidal heating and the presence of a deep ocean at various stages of the history of Miranda, as well as global differentiation (Castillo-Rogez et al., 2023), would have erased open porosity in the moon.

The parameter range (density, thickness) of the two-layer models and of models including potential internal ocean was investigated (Castillo-Rogez et al., 2023). A pure-ice mantle (920 kg/m^3) gives a good agreement with observed elongation of Miranda and Ariel although a range of densities is possible (Castillo-Rogez et al., 2023). Assumed core densities span a range that covers solar composition (Néri et al., 2020; Reynard and Sotin, 2023) containing carbonaceous matter mixed with hydrous and anhydrous silicates and sulfides (2300 and 3150 kg/m^3), and carbon-free hydrous and anhydrous silicates and sulfides (3150 and 3750 kg/m^3). Core densities below 3400 kg/m^3 are compatible with current constraints (Castillo-Rogez et al., 2023), making only anhydrous carbon-poor compositions unlikely.

The power-law radius-density relationship for Uranus moons suggests that a specific mechanism fractionated ice and rock and controlled the composition of moons during accretion from the disk (Fig. 1b). Assuming that porosity is negligible as argued above, a two-component mixture of pure ice shell and a refractory core of variable densities (Fig. S1) yield a refractory core weight fraction that varies linearly with the log of the moon radius. Changing the rock density only changes the slope of the relationship because component density is almost constant at the pressures and temperatures of Uranian moons (Castillo-Rogez et al., 2023; Hussmann et al., 2006).

3. Ice-rock fractionation

3.1. Differential diffusion

Out of the possible mechanisms, differential diffusion of silicate and ice grains in the disk has been studied using dynamical models (Woo et al., 2022). A diffusion profile develops in the disk simulation (Fig. 2a) near the ice line where small silicate grains are lost due to gas drag with respect to larger ice grains. Typical one-dimensional diffusion profiles can be fitted with:

$$\left(\frac{C^{ice}}{C^{rock}}\right)_r = \left(\frac{C^{ice}}{C^{rock}}\right)_0 \operatorname{erfc}\left(\frac{r}{2\sqrt{\mathrm{D}t}}\right) \quad (1),$$

where *t* is time, D is the diffusion coefficient, and *r* the orbital distance. A diffusion profile described by equation (1) develops in a disk simulation (Woo et al., 2022) due to gas drag that affects only small silicate particles and not large ice grains. This diffusion profile is reflected in the bulk model moon composition (Fig. 2a). The diffusion profile defined by moon composition is broader than that in the disk because moon accretion gathers material from a large region. Model A2A (Woo et al., 2022) accounts for Miranda's rock-poor composition.

The overall fit of equation (1) to the A2A model moon composition (Woo et al., 2022) is good, but the fit to actual densities of Uranus moons is mediocre (Fig. 2a). In particular, the data for Ariel and Umbriel are not well accounted for by diffusion, because they would have to form in the same region in the diffusion profile to have a similar composition before moving apart from each other. Including turbulence-driven diffusion in the models does not improve the match, as it produces small dense satellites and relatively light large satellites and no systematic size-density relationship (Woo et al., 2022). The power-law between density and size Fig. 1b is also not well reproduced, suggesting a different mechanism is at work.

3.2. Closed-system Rayleigh fractionation

N-body simulations (Ida et al., 2020; Woo et al., 2022) of moon formation assume a closed system since all the mass of condensed solids is used to make the satellites. Small inner moons and rings represent a negligible 0.05% of satellite mass. The evolution of composition associated with fractionation of components, here ice and rock, can be described as an incremental process called distillation where a condition of equilibrium is applied at each step (Rayleigh, 1896).

The initial reservoir, i.e. the condensed solids in the disk that will accrete to form the moons, has a size equal to the total mass of the moons ($M \sim 10^{-4}\ M_U$) and a homogeneous ice/rock ratio $\left(\frac{M_{ice}}{M_{rock}}\right)$, where M_{ice} and M_{rock} are the initial mass of ice and rock, respectively. The rock component is composed of all potential refractory phases (*e.g.*, silicates, sulfides, carbonaceous matter). A constant fractionation of ice and rock is assumed at each step during the accretion of the moons:

$$\left(\frac{dm_{rock}^{acc}}{dm_{ice}^{acc}}\right) = \mathrm{F}\left(\frac{m_{rock}^{disk}}{m_{ice}^{disk}}\right) \qquad (2),$$

where F is the fractionation constant between the accreted material in moons (suffix *acc*) and the material that is still in the disk (suffix *disk*), m_j^{disk} is the mass of material j (j=rock, ice) remaining in the disk, and dm_j^{acc} is the elementary accreted mass that forms the growing moon. Note that this process leads to an initial layered structure with, for F larger than 1, lighter layers forming the outer shells of the moon as the disk gets more and more depleted in rocks. The conservation of mass implies:

$$m_{ice}^{acc} + m_{ice}^{disk} = M_{ice},$$

$$m_{rock}^{acc} + m_{rock}^{disk} = M_{rock},$$

which leads to $dm_{ice}^{acc} = -dm_{ice}^{disk}$ and $dm_{rock}^{acc} = -dm_{rock}^{disk}$. Using these equalities into equation (2) yields:

$$\left(\frac{dm_{rock}^{disk}}{dm_{ice}^{disk}}\right) = \mathrm{F}\left(\frac{m_{rock}^{disk}}{m_{ice}^{disk}}\right) \qquad (3),$$

which can be written

$$\left(\frac{dm_{rock}^{disk}}{m_{rock}^{disk}}\right) = \mathrm{F}\left(\frac{dm_{ice}^{disk}}{m_{ice}^{disk}}\right), \text{ or } dLn\left(m_{rock}^{disk}\right) = F.dLn\left(m_{ice}^{disk}\right) \qquad (4).$$

With the initial conditions, the solution of equation (4) is:

$$\left(\frac{m_{rock}^{\mathrm{disk}}}{M_{rock}}\right) = \left(\frac{m_{ice}^{\mathrm{disk}}}{M_{ice}}\right)^{F} \qquad (5).$$

If F>1, the disk gets depleted in rocks and enriched in ice. Conversely, the icy moons are enriched in rocks compared to the disk.

Similar equations have been derived to describe the evolution of elemental or isotopic compositions of rocks and meteorites in geo- and cosmochemistry (Albarède, 1995). Following this approach, we can rewrite equation (5) as:

$$\left(\frac{C_{rock}^{disk}}{C_{ice}^{disk}}\right) = \left(\frac{C_{rock}^{0}}{C_{ice}^{0}}\right) z^{\mathrm{F}-1} \qquad (6),$$

where C_j^{disk} is the mass fraction of a given component (j=rock or ice) in the disk, C_j^0 is the initial concentration in the disk, and z is defined as:

$$z = f_{disk} C_{ice}^{disk} / C_{ice}^{0} \qquad (7),$$

where f_{disk} is the fraction of residual material in the disk ($f_{disk} = \frac{m_{ice}^{disk} + m_{rock}^{disk}}{M}$). z is also the ratio of ice remaining in the disk to the initial mass of ice ($z = {m_{ice}^{disk}}/{M_{ice}}$).

The initial rock/ice ratio $\left(\frac{C^0_{rock}}{C^0_{ice}}\right)$ depends on the assumed nature and density of the refractory component:

$$\left(\frac{C^0_{rock}}{C^0_{ice}}\right) = \frac{\rho_{rock}}{\rho_{ice}}\frac{\rho-\rho_{ice}}{\rho_{rock}-\rho} \qquad (8),$$

with ρ the density of the system ($\rho = \frac{\sum M_{sat}}{\sum V_{sat}} = 1616\ kg/m^3$). Using solar rock densities of 2300 and 3150 kg/m^3, and ice density of 920 kg/m^3, yields initial rock/ice ratios of 2.55 and 1.55, respectively. The rock/ice ratio is used to calculate at each step of the distillation process the density ρ_s of the accreted solids:

$$\rho_s = \frac{\rho_{rock}\rho_{ice}}{\rho_{rock}C^{acc}{}_{ice}+\rho_{ice}C^{acc}{}_{rock}} \qquad (9).$$

Densities of accreting solids obtained from equations (2-9) are reported for a chosen fractionation coefficient F of 1.3 favoring fractionation of refractories of assumed density of 2300 kg/m^3 with respect to ice in accreted solids (Fig. 2b). Changing the density of the refractory component requires a small adjustment of the F value to match the moon densities (Fig. S2) from 1.3±0.05 to 1.25±0.05 for rock densities of 2300 and 3150 kg/m^3, respectively.

As accretion proceeds, the fraction f_{disk} of material in the disk and the density (or the rock/ice ratio) of the accreting solids decreases. In this scenario, moons accreted in order of decreasing density, first Oberon and Titania, then Umbriel and Ariel, and finally Miranda. The density of the moons forming by this process is obtained as the integrated density (equation 8) of solid accreted over a fraction f_{disk} corresponding to the fractional mass of the moon, or pair of moons forming simultaneously (*i.e.*, with similar density). It implies the moons feed from homogenized or large regions of the disk, as is the case during growth by planetesimal accretion as discussed in section 3.1 (Fig. 2a). Diffusion affects the refractory/ice ratio both spatially and in time whereas in the Rayleigh fractionation model, the composition is spatially homogeneous and varies only through time.

More complex systems with all moons accreting until the disk vanishes, partially overlapping windows or F varying with time are possible, but we tested only the simplest model with one adjustable variable F given the scarcity of constraints (three resolved density values). Thus we assumed Oberon and Titania accreted over the same time interval corresponding to their aggregate mass (71.4% of the disk mass) and then migrated outwards the accreting disk due to tidal friction within Uranus, a process similar to that invoked to explain the outward migration of the saturnian moons(Lainey et al., 2020). Umbriel and Ariel (27.9% of the disk mass) then accreted simultaneously within the remaining disk before Miranda accreted the remaining (0.7%) disk material (Fig 2b). Average densities over the three accretion periods agree within uncertainties with those of the corresponding moons over a narrow range of F values of 1.2-1.35 (Fig. S2), corresponding to an enrichment in refractory of <10% in accreted solids with respect to the disk.

4. Discussion

4.1. Mechanisms of ice-rock fractionation

Rayleigh fractionation accounts for the density-radius power law in Uranian moons, if there exists a mild initial enrichment in refractory component (7-11%) of incrementally accreted solids with respect to disk solids, that progressively increases to 20%. Co-accretion of silicates and ice beyond the ice line into pebbles is a common way for explaining the accretion of ice-rock mixtures. Fractionation could occur during pebble formation, but ice pebbles grow easier than silicate pebbles because their cohesion is higher (Woo et al., 2022). With current pebble formation models, first-formed pebbles should be ice-enriched, in contradiction with first accreting solids enriched in refractories (F>1) assumed here. Carbonaceous particles that could be both sticky and cohesive are overlooked in current models and may favor accretion of the refractory component in pebbles.

If fractionation is not associated with pebble formation, it may occur during oligarchic growth of moons by small body accretion. In the Uranian disk, "satellitesimals and satellites must be formed in situ" because growth is much faster than drift in a gas-depleted disk (Ida et al., 2020). N-body simulations using final disk density distribution yield results that reproduces the mass-orbit configuration of the Uranian satellites, and follow an oligarchic growth model (Ida et al., 2020; Kokubo and Ida, 1998). Shocks during the accretion process can remove preferentially ice if it reaches its sublimation temperature (Nimmo and Korycansky, 2012). Taking into account orbital velocities of Uranian satellites, impact velocities up to 6-12 km/s are obtained (Zahnle et al., 2003), while minimum velocities are given by the escape velocities of 0.8-1.1 km/s for the large Uranian satellites. Parametric analysis of numerical simulations of impacts (Kraus et al., 2011) indicate that a mass of ice of 0-100% the mass of the impactor is vaporized for this velocity range. It accounts for fractionation factor in the range F=1.2-1.35, with initial rock enrichment of 7-11% requiring velocities of 2.4-4.7 km/s. Quantitative estimates of F should take into account precise velocity distribution during accretion, ice loss by ablation of planetesimals (Ronnet and Johansen, 2020) or by shocks, and require further modeling combining thermodynamics, shock physics and N-body simulations. Early ice-rock differentiation on growing planetesimals due to deformation and heating induced by shocks during accretion events may facilitate this scenario. Subsequent shocks could erode an upper ice-enriched shell and redistribute preferentially ice into the disk, leaving a higher proportion of rocks in accreted solids.

Rayleigh fractionation better accounts for the observed density of Uranus regular moons than diffusion (Figs. 1b and 2b). Differential diffusion does not reproduce well the power-law between size and density of Uranian moons. These mechanisms are not exclusive as they result in concurrent patterns of increasing moon density with increasing mass and orbital radius. Rayleigh fractionation mechanisms need to be tested with N-body simulations. Rayleigh fractionation requires sequential growth of satellites, which may be achieved by outward drift of satellites growing from the disk and retrieval from the feeding zone. Outward tidal drift and sequential growth is predicted in simulations of the formation of inner Saturnian satellites (see Figs. 3 and 6 in Charnoz et al. (2011).

4.2. Consequences for moon formation

With moon composition resulting from Rayleigh distillation, the power-law between density and size may be understood since the evolution of accreting solid density with respect to the accreted fraction is close to a power-law (Fig. 2a), except at very low f_{disk} (<0.0005) that have a negligible contribution to the final budget. The slope of the power-law relationship for the moons is however higher than that followed by the accreting solids. This is due to the fact that moons are accreted over finite windows of diminishing size with time when the distillation curve follows the incremental evolution. Also, Titania-Oberon and Ariel-Umbriel form two pairs of similar size and density, while Miranda's size and density are unique. Such pairs of large satellites of similar size and unique small satellites are a result of oligarchic growth model of Uranian satellites (see Fig. 1 in Ida et al., 2020) and do not require fractionation or diffusion. The actual slope of the power-law between size and density thus results both from ice/rock fractionation and the oligarchic growth process. Effects of Rayleigh fractionation can be deciphered in Uranus regular moons likely because they formed in a single stage event from a closed-system disk.

Fractionation of rock and ice during accretion of planets and moons is likely not restricted to the Uranus' system, and may occur in other planetary disks. Rayleigh distillation due to ice-rock fractionation in the Saturnian disk may for instance account for the puzzling ice-rich compositions of Rhea and Tethys, and the pure ice nature of Saturn's rings. It cannot however explain the erratic pattern of Saturnian moon density as a function of orbital distance

(Fig. 1a), and the absence of power-law relationship between density and radius among these moons. Rayleigh fractionation adds to mechanisms affecting the composition of accreting planets and moons in disks such as temporal/spatial variation of disk composition due to diffusion and turbulence in open system boundary conditions (Birnstiel et al., 2010; Youdin and Lithwick, 2007), capture and fragmentation (Asphaug and Reufer, 2013; Ronnet and Johansen, 2020), etc. In the complex moon system of Saturn, a combination of these mechanisms was likely, hampering recognition of Rayleigh fractionation alone. Around Jupiter, chemical zoning is currently ascribed to moon formation on both sides of the ice line in the circumplanetary disk (Ronnet et al., 2017), tidal heating (Canup and Ward, 2009), and may also have been affected by the migration of Jupiter (Lubow et al., 1999).

4.3. Implications for outer solar system objects and Uranian moon composition

Composition of ice/carbon-rich bodies in the solar system involves three major components, ice and water bound in minerals (IC*), dry chondritic silicates-sulfides (SSC*), and carbonaceous matter (COM), and suggest the existence of a composition continuum (Fig. 3) including carbonaceous chondrite (CI) and cometary compositions (Reynard and Sotin, 2023). The COM-free end-members of the continuum is a hydrated silicate SSC corresponding to a mixture of SSC* and about 10% of H_2O (as ice or as hydrated minerals) with a density of 3150 kg/m^3, and the SSC-free component a mixture of about 70% of ice and 30% COM with density of 1050 kg/m^3.The origin of such a compositional zoning in the solar system may be ascribed to Rayleigh fractionation or temperature zoning favoring condensation of ices and organic matter at larger distances from the Sun.

Fractionation in Uranian moons can be modeled by mixing either refractories with pure ice or along the CI-comet continuum (Fig. 3). Starting from the whole system composition and density of 1616 kg/m^3, mixing with pure ice implies constant core densities of about 2500 kg/m^3 at constant SSC/COM ratio in all Uranian moons, starting from compositions close to that inferred for Enceladus (Reynard and Sotin, 2023). Such core densities are consistent with dominantly hydrated silicate mineralogy. On the other hand, mixing along the CI-comet would involve decreasing core density as COM/SSC ratio increases, ending with a core density of 1800 kg/m^3 for Miranda. Both are consistent with the current loose constraints on inner models from bulk density and shape (Castillo-Rogez et al., 2023). Measurement of moons' reduced moment of inertia (RMI) by a mission to the Uranus system (National Academies of Sciences Engineering and Medicine, 2022) would help determine which of the two possibilities works best, if any, assuming it could resolve a difference between RMI of 0.339 and 0.351 for Miranda, and of 0.325 and 0.331 for Ariel.

Acknowledgements. Constructive comments from two anonymous referees helped improve the manuscript. This work was supported by Institut National des Sciences de l'Univers through Programme National de Planétologie, by the Agence Nationale de la Recherche (ANR, project OSSO BUCO, ANR-23-CE49-0003) and by the European Union (ERC, PROMISES, project #101054470). Views and opinions expressed are however those of the authors only and do not necessarily reflect those of the European Union or the European Research Council. Neither the European Union nor the granting authority can be held responsible for them.

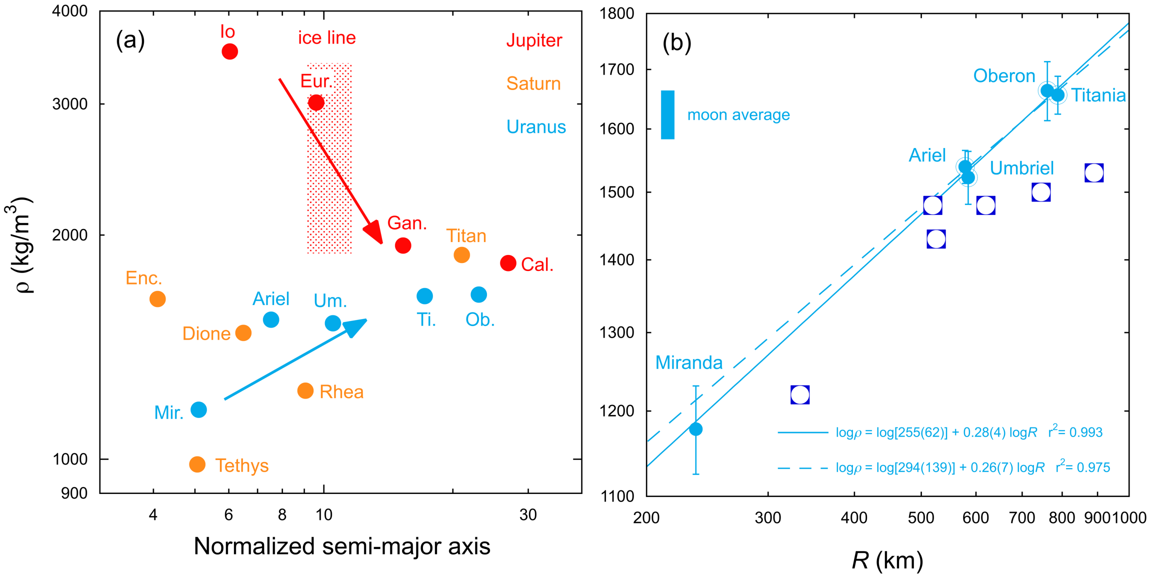

Fig. 1. a) Density of giant planets' moons as a function of orbital semi-major axis normalized to planet radius (NSMA). Jupiter moons' density decreases with increasing NSMA (red arrow), a variation attributed to the crossing of the ice-line that inhibits ice accretion close to the planet, or by ice loss due to tidal or radiative heating. In the opposite, Uranus moons' density increases with increasing NSMA (blue arrow). These patterns reflect different formation mechanisms of moons in the Uranian and Jovian systems. Saturn moons show an erratic pattern, that likely reflects a complex history. b) Uranus moon density as a function of moon radius *R* evidences a power-law relationship. The linear fit is similar whether Miranda is included (full line and symbols) or not (dashed line and empty symbols). Uncertainties on last digits of fitted parameters are shown in parentheses. Dark blue symbols represent six moons predicted from N-body simulation of growth from an ice and silicate disk (prefered model A2A in Woo et al., 2022).

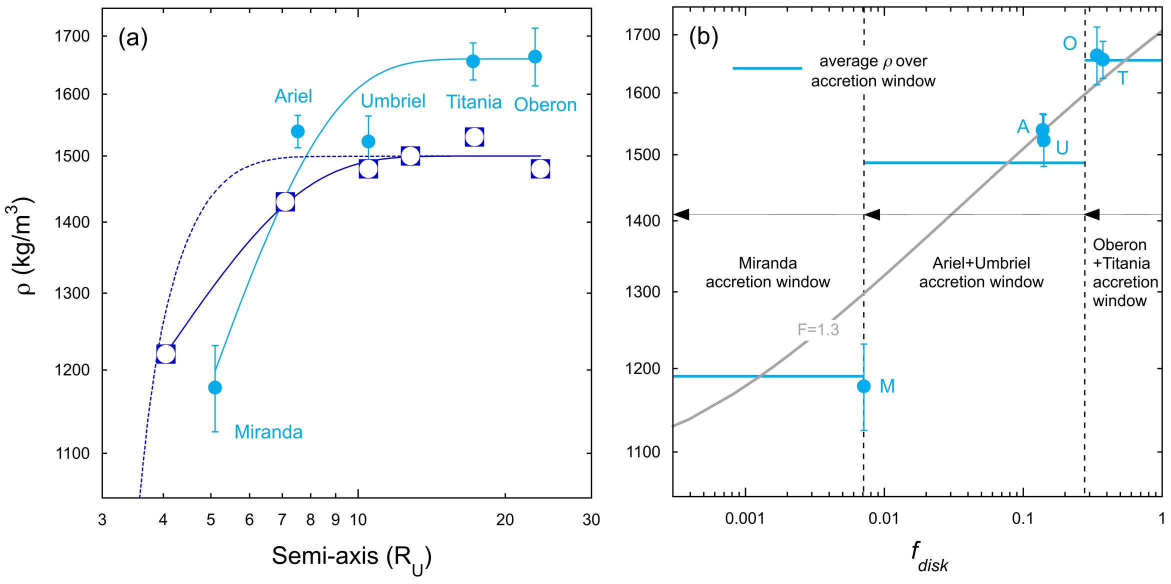

Fig. 2. Fractionation mechanisms accounting for varying densities in Uranian moons: a) Differential diffusion in the disk yields varying density of solids as a function of semi-axis orbital distance (R_U = 25362 km, radius of Uranus). Diffusion equation (1) fits simulated dust/pebble composition (dashed curve, assumed starting density of 1500 kg/m^3) for the A2A disk model (Woo et al., 2022). Moon compositions formed from the same disk by hierarchical aggregation of planetesimals show a milder diffusion profile (dark blue squares and solid curve, $r^2 = 0.91$), indicating that the feeding zone of moons is broad and involve mixing over distances of several R_U units. Diffusion equation does not account well for the actual compositions of Ariel and Umbriel (light blue curve and symbols, $r^2 = 0.78$), unless this pair of satellites formed at neighboring semi-axis before migrating apart from each other. b) Rayleigh fractionation (grey curve, equations 2-9 for fractionation factor F=1.3) gives results close to a power-law relation between density and mass fraction of residual solids in the disk (f_{disk}), except at very low f_{disk}. Average compositions (light blue lines) over successive accretion windows (arrows) match those of the moons (light blue symbols). Oberon-Titania pair formed first followed by Ariel-Umbriel pair, before Miranda accreted from the rock-poor leftovers. The model assumes mixing over long distances in the disk at the pebble or at the planetesimal aggregation stages.

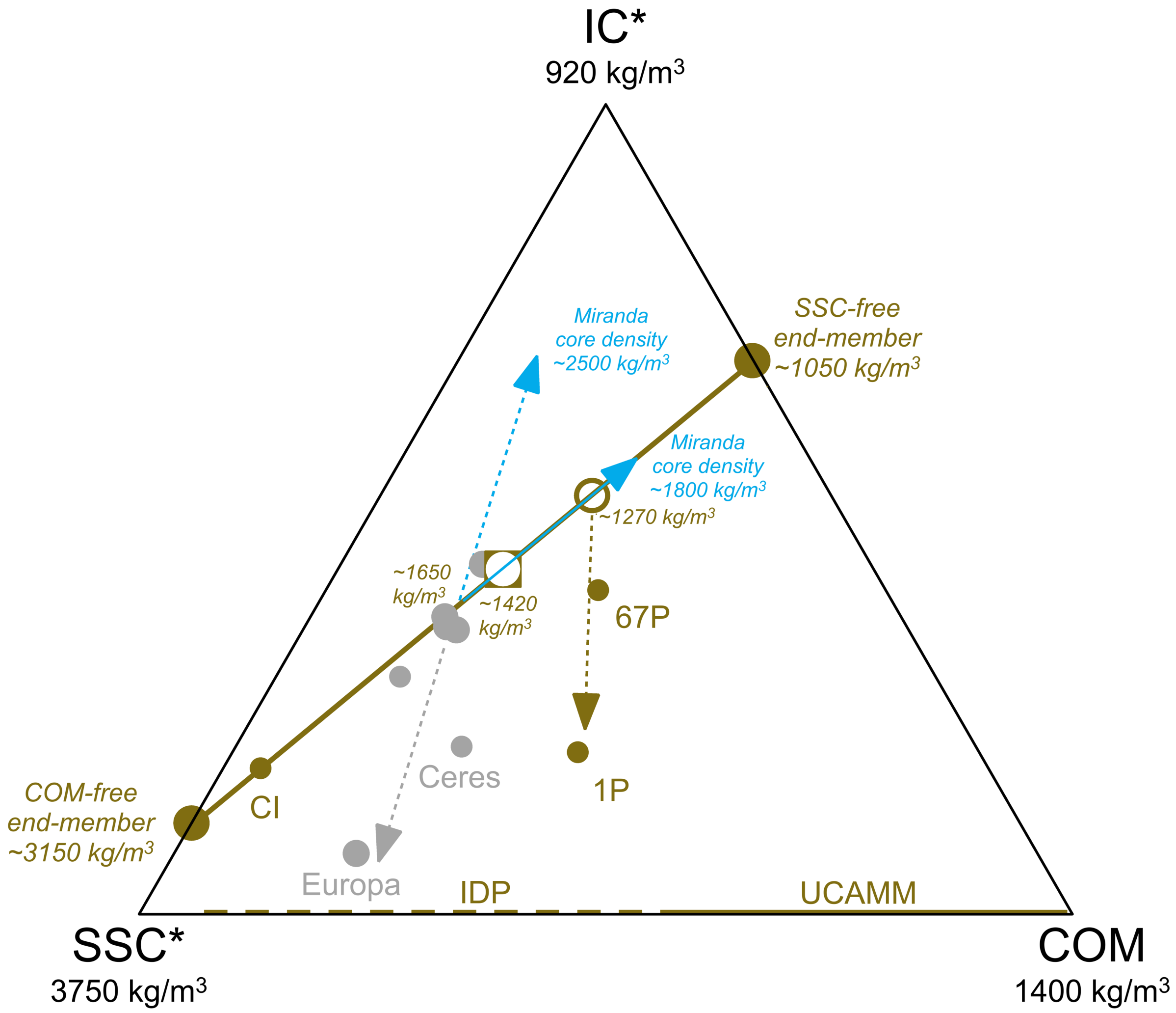

Fig. 3. Possible compositions of Uranian moons in a ternary diagram for icy body composition in the outer solar system (modified from Reynard and Sotin, 2023). SSC* is a dry silicate-sulfide component, COM carbonaceous matter, and IC* the ice component. Indicative densities of components are given. Solar composition (Lodders, 2021) is represented by the brown square with hollow center. It defines a CI-solar continuum (brown line) passing through the CI-chondrite composition (small brown circle), and extrapolated to COM-free and SSC-free end-members (large brown circles). Grey points represent icy body compositions. Those close to the CI-comet continuum are Enceladus, Dione, Ganymede, Titan and Haumea. The blue arrows show the effect of Rayleigh fractionation on Uranus moon composition, either between a refractory and pure ice component (dashed, constant core density of ~2500 kg/m^3 in moons with subsolar C/Si ratio) or along the CI chondrite-solar-cometary continuum (solid, decreasing moon core density down to ~1800 kg/m^3 in Miranda). The grey arrows represent the trend for an ice-depleted body like Europa near the snow line (Mousis et al., 2023), and the brown dashed line ice sublimation for comets (1P and 67P). IDP and UCAMM grains represent fully sublimated samples of the CI-solar-comet continuum. Inferred initial comet composition is given by the open brown circle on the CI-solar continuum.

Table 1. Physical Properties of Uranus' Regular Moons (Jacobson (2014); figures in parentheses give the 1σ uncertainty on the last digits).

Properties	Miranda	Ariel	Umbriel	Titania	Oberon
Mean radius (km)	235.8(7)	578.9(6)	584.7(2.8)	788.9(1.8)	761.4(2.6)
Mean density (kg/m^3)	1178(53)	1539(26)	1523(41)	1656(32)	1664(50)

References

Albarède, F., 1995. Introduction to Geochemical Modeling. Cambridge University Press, Cambridge.

Asphaug, E., Reufer, A., 2013. Late origin of the Saturn system. Icarus 223, 544-565.

Beddingfield, C.B., Leonard, E., Cartwright, R.J., Elder, C., Nordheim, T.A., 2022. High Heat Flux near Miranda's Inverness Corona Consistent with a Geologically Recent Heating Event. The Planetary Science Journal 3, 174.

Bierson, C.J., Nimmo, F., 2022. A note on the possibility of subsurface oceans on the uranian satellites. Icarus 373, 114776.

Birnstiel, T., Dullemond, C.P., Brauer, F., 2010. Gas- and dust evolution in protoplanetary disks. Astronomy & Astrophysics 513.

Boué, G., Laskar, J., 2010. A collisionless scenario for Uranus tilting. The Astrophysical Journal Letters 712, L44.

Canup, R.M., Ward, W.R., 2009. Origin of Europa and the Galilean Satellites, in: Pappalardo, R., McKinnon, W.B., Khurana, K.K. (Eds.), Europa, p. 59.

Castillo-Rogez, J., Weiss, B., Beddingfield, C., Biersteker, J., Cartwright, R., Goode, A., Melwani Daswani, M., Neveu, M., 2023. Compositions and Interior Structures of the Large Moons of Uranus and Implications for Future Spacecraft Observations. Journal of Geophysical Research: Planets 128, e2022JE007432.

Charnoz, S., Crida, A., Castillo-Rogez, J.C., Lainey, V., Dones, L., Karatekin, Ö., Tobie, G., Mathis, S., Le Poncin-Lafitte, C., Salmon, J., 2011. Accretion of Saturn's mid-sized moons during the viscous spreading of young massive rings: Solving the paradox of silicate-poor rings versus silicate-rich moons. Icarus 216, 535-550.

Ćuk, M., El Moutamid, M., Tiscareno, M.S., 2020. Dynamical History of the Uranian System. The Planetary Science Journal 1, 22.

Hussmann, H., Sohl, F., Spohn, T., 2006. Subsurface oceans and deep interiors of medium-sized outer planet satellites and large trans-neptunian objects. Icarus 185, 258-273.

Ida, S., Ueta, S., Sasaki, T., Ishizawa, Y., 2020. Uranian satellite formation by evolution of a water vapour disk generated by a giant impact. Nature Astronomy 4, 880-885.

Jacobson, R.A., 2014. The orbits of the Uranian sattelites and rings, the gravity field of the Uranian system, and the orientation of the pole of Uranus. The Astronomical Journal 148, 76.

Kegerreis, J.A., Teodoro, L.F.A., Eke, V.R., Massey, R.J., Catling, D.C., Fryer, C.L., Korycansky, D.G., Warren, M.S., Zahnle, K.J., 2018. Consequences of Giant Impacts on Early Uranus for Rotation, Internal Structure, Debris, and Atmospheric Erosion. The Astrophysical Journal 861, 52.

Kokubo, E., Ida, S., 1998. Oligarchic Growth of Protoplanets. Icarus 131, 171-178.

Kraus, R.G., Senft, L.E., Stewart, S.T., 2011. Impacts onto H2O ice: Scaling laws for melting, vaporization, excavation, and final crater size. Icarus 214, 724-738.

Kurosaki, K., Inutsuka, S.-i., 2019. The Exchange of Mass and Angular Momentum in the Impact Event of Ice Giant Planets: Implications for the Origin of Uranus. The Astronomical Journal 157, 13.

Lainey, V., Casajus, L.G., Fuller, J., Zannoni, M., Tortora, P., Cooper, N., Murray, C., Modenini, D., Park, R.S., Robert, V., Zhang, Q., 2020. Resonance locking in giant planets indicated by the rapid orbital expansion of Titan. Nature Astronomy 4, 1053-1058.

Lainey, V., Rambaux, N., Tobie, G., Cooper, N., Zhang, Q., Noyelles, B., Baillié, K., 2024. A recently formed ocean inside Saturn's moon Mimas. Nature 626, 280-282.

Lodders, K., 2021. Relative Atomic Solar System Abundances, Mass Fractions, and Atomic Masses of the Elements and Their Isotopes, Composition of the Solar Photosphere, and

Compositions of the Major Chondritic Meteorite Groups. Space Science Reviews 217, 44.

Lubow, S.H., Seibert, M., Artymowicz, P., 1999. Disk Accretion onto High-Mass Planets. The Astrophysical Journal 526, 1001.

Mousis, O., Schneeberger, A., Lunine, J.I., Glein, C.R., Bouquet, A., Vance, S.D., 2023. Early Stages of Galilean Moon Formation in a Water-depleted Environment. The Astrophysical Journal Letters 944, L37.

National Academies of Sciences Engineering and Medicine, 2022. Origins, Worlds, and Life: A Decadal Strategy for Planetary Science and Astrobiology 2023-2032. The National Academies Press, Washington, DC.

Néri, A., Guyot, F., Reynard, B., Sotin, C., 2020. A carbonaceous chondrite and cometary origin for icy moons of Jupiter and Saturn. Earth and Planetary Science Letters 530, 115920.

Neveu, M., Rhoden, A.R., 2019. Evolution of Saturn's mid-sized moons. Nature Astronomy 3, 543-552.

Nimmo, F., Korycansky, D.G., 2012. Impact-driven ice loss in outer Solar System satellites: Consequences for the Late Heavy Bombardment. Icarus 219, 508-510.

Rayleigh, L., 1896. Theoretical considerations respecting the separation of gases by diffusion and similar processes. The London, Edinburgh, and Dublin Philosophical Magazine and Journal of Science 42, 493-498.

Reinhardt, C., Chau, A., Stadel, J., Helled, R., 2020. Bifurcation in the history of Uranus and Neptune: the role of giant impacts. Monthly Notices of the Royal Astronomical Society 492, 5336-5353.

Reynard, B., Sotin, C., 2023. Carbon-rich icy moons and dwarf planets. Earth and Planetary Science Letters 612, 118172.

Ronnet, T., Johansen, A., 2020. Formation of moon systems around giant planets. A&A 633.

Ronnet, T., Mousis, O., Vernazza, P., 2017. Pebble Accretion at the Origin of Water in Europa. The Astrophysical Journal 845, 92.

Saillenfest, M., Rogoszinski, Z., Lari, G., Baillié, K., Boué, G., Crida, A., Lainey, V., 2022. Tilting Uranus via the migration of an ancient satellite. A&A 668.

Slattery, W.L., Benz, W., Cameron, A.G.W., 1992. Giant impacts on a primitive Uranus. Icarus 99, 167-174.

Szulágyi, J., Cilibrasi, M., Mayer, L., 2018. In Situ Formation of Icy Moons of Uranus and Neptune. The Astrophysical Journal Letters 868, L13.

Thomas, P.C., 1988. Radii, shapes, and topography of the satellites of Uranus from limb coordinates. Icarus 73, 427-441.

Woo, J.M.Y., Reinhardt, C., Cilibrasi, M., Chau, A., Helled, R., Stadel, J., 2022. Did Uranus' regular moons form via a rocky giant impactor? Icarus 375, 114842.

Youdin, A.N., Lithwick, Y., 2007. Particle stirring in turbulent gas disks: Including orbital oscillations. Icarus 192, 588-604.

Zahnle, K., Schenk, P., Levison, H., Dones, L., 2003. Cratering rates in the outer Solar System. Icarus 163, 263-289.

Supplementary information

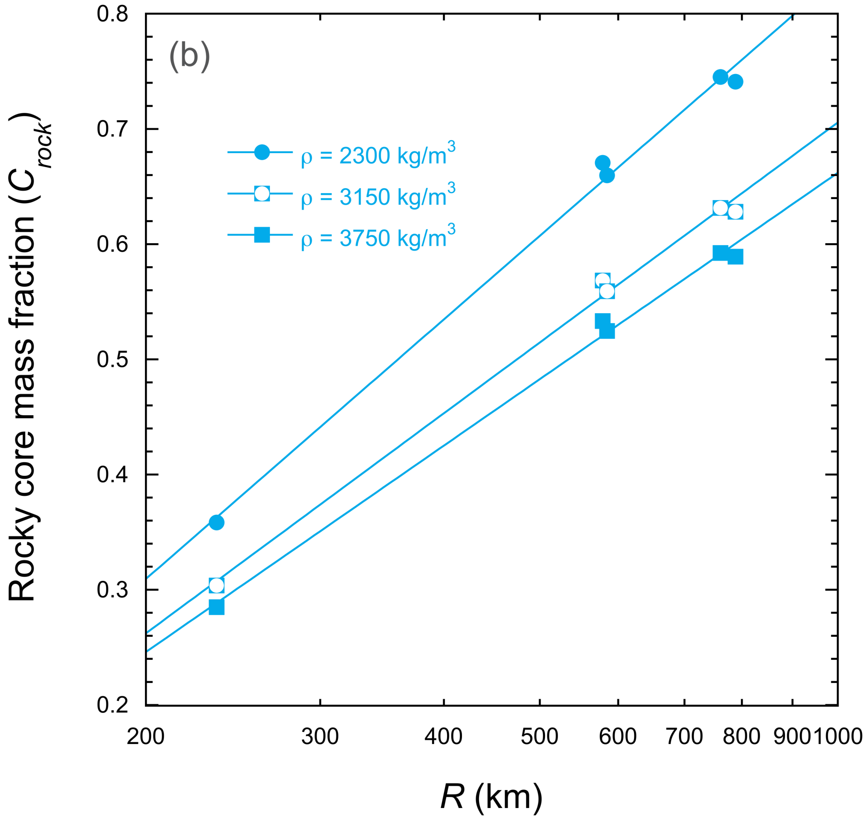

Fig. S1. Mass fraction of the refractory core assuming various rock densities or mineralogies of 2300 kg/m^3 (hydrous silicate-sulfide and carbonaceous matter), 3150 kg/m^3 (wet silicate-sulfide and carbonaceous matter), and 3750 kg/m^3 (carbon-free dry silicate-sulfide).

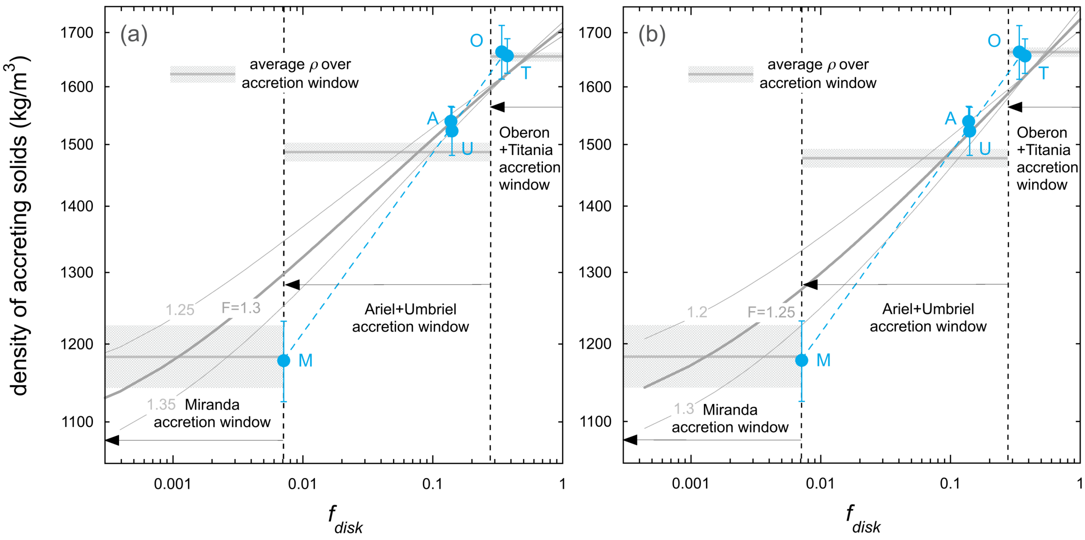

Figure S2. Influence of density on fractionation constant F. Rayleigh fractionation curves during accretion for rock density of a) 2300 kg/m^3, and b) 3150 kg/m^3. Moon densities are reproduced for constant F values of 1.3±0.05 and 1.25±0.05, respectively, hence large variations of refractory density have a small effect on F.